Nanoscale

Accepted Manuscript

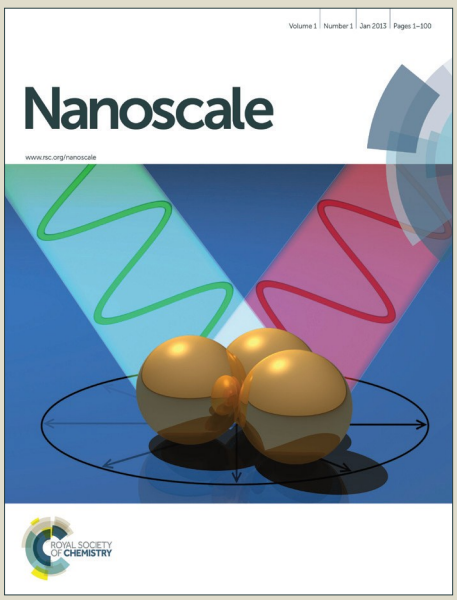

ROYAL SOCIETY OF CHEMISTRY

www.rsc.org/nanoscale

Nanoparticle-enhanced Synergistic HIFU Ablation and Transarterial Chemoembolization for Efficient Cancer Therapy

Yufeng You,,[1,2]Zhigang Wang,[1] Haitao Ran,[1]Yuanyi Zheng,[1] Dong Wang,[3] Jinshun Xu,[1] Zhibiao Wang,[4] Yu Chen[5] and Pan Li[1**]*

[1]Institute of Ultrasound Imaging & Department of Ultrasound, the Second Affiliated Hospital of Chongqing Medical University, Chongqing Key Laboratory of Ultrasound Molecular Imaging, Chongqing, 400010, P. R. China. E-mail: cqlipan@163.com

[2]Department of Radiology, Central Hospital of Enshi Autonomous Prefecture, Hubei, 445000, P. R. China.

[3]Department of Ultrasound, Children's Hospital Affiliated to Chongqing Medical University, Chongqing, 400014, P. R. China.

[4]College of Biomedical Engineering, Chongqing Medical University, Chongqing, 400016, P. R. China

[5]State Key Laboratory of High Performance Ceramics and Superfine Microstructure, Shanghai Institute of Ceramics, Chinese Academy of Sciences, Shanghai, 200050, P. R. China. Email: chenyu@mail.sic.ac.cn

Abstract

High intensity focused ultrasound (HIFU) is being generally explored as a non-invasive therapeutic modality to treat solid tumors. However, the clinical use of HIFU for large and deep tumor-ablation applications such as hepatocellular carcinoma (HCC) is currently entangled with long treatment duration and high operating energy. This critical issue can be potentially resolved by the introduction of HIFU synergistic agents (SAs). Traditional SAs such as microbubble and microparticles face the problem of big size, short cycle time, the damage of mononuclear phagocytic system and unsatisfied targeting efficiency. In this work, we have developed a facile and versatile nanoparticle-based HIFU-synergistic cancer surgery enhanced by transarterial chemoembolization for high-efficient HCC treatment based on elaborately designed Fe_3O_4-PFH/PLGA nanocapsules. Multifunctional Fe_3O_4-PFH/PLGA nanocapsules were administrated into tumor tissues *via* transarterial injection combined with Lipiodol to achieve high tumor accumulation because transarterial chemoembolization by Lipiodol could block the blood vessels. The high synergistic HIFU-ablation effect was successfully achieved against HCC tumors based on the phase-transformation performance of perfluorohexane (PFH) inner core in the composite nanocapsules, as systematically demonstrated in VX2 liver-tumor xenograft in rabbits. Multifunctional Fe_3O_4-PFH/PLGA nanocapsules were also demonstrated as the efficient contrast agents for ultrasound, magnetic resonance and photoacoustic tri-modality imagings, potentially applicable for imaging-guided HIFU synergistic surgery. Therefore, the elaborate integration of traditional transarterial chemoembolization with recently developed nanoparticle-enhanced HIFU cancer surgery could efficiently enhance the HCC cancer-treatment outcome, initiating a new and efficient therapeutic protocol/modality for clinic cancer treatment.

Keywords. Nanomedicine, HIFU, Transarterial chemoembolization, Synergistic therapy, Cancer.

Table of Content

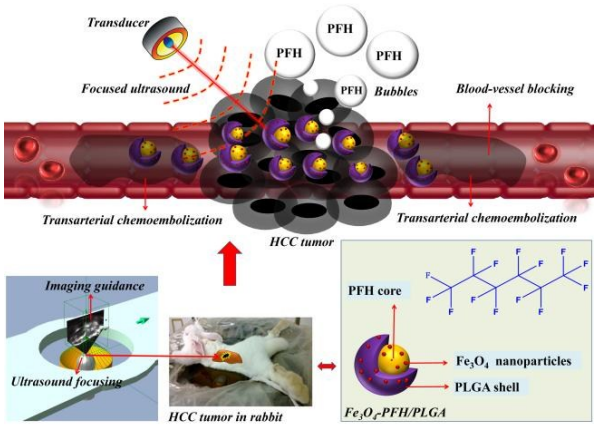

1. Introduction

Hepatocellular carcinoma (HCC) is a common type of malignant tumor in humans.[1] Most of HCC patients lost the opportunity of surgery because of limited number of liver donors, accompanied with inoperable diseases. Recently, minimally-invasive and imaging-guided tumor-ablation techniques have been quickly developed for efficient management of HCC.[2] Such an imaging-guided ablation technique offers superior characteristics such as substantially reduced mortality and therapeutic complication, shortened hospital stays, and corresponding improved life quality. Several representative minimally-invasive therapies have been clinically developed for the therapy of inoperable HCC, including transarterial chemoembolization, radiofrequency waves, microwaves, lasers and cryogens.[3-8]

Among aforementioned therapeutic modalities, transarterial chemoembolization is one of the most important treating protocols for the unresectable HCC. Since its inception in the early 80s, this technique has been developed based on the use of the iodinated oil Lipiodol.[9] Lipiodol is clinically employed not only for its radiopaque properties but also for its drug-delivery and tumor-seeking performance. Lipiodol is also featured with intriguing capability to induce plastic and transient embolization of the tumor microcirculation, which is adapted to the size of blood vessels.[10] However, viable tumor cells still remain after transarterial chemoembolization, which can cause local tumor recurrence and further distant metastasis,[11] leading to the failure of transarterial chemoembolization. In this regard, supplementary therapeutic modalities are generally introduced to enhance the therapeutic efficiency of transarterial chemoembolization, such as chemotherapy, radiofrequency and ultrasound treatment.

High-intensity focused ultrasound (HIFU) is generally regarded as the non-invasive extracorporal ablation technology that focuses the high-intensity ultrasound energy to ablate and destroy the tumor cell/tissue. Compare with the typical cancer-treatment protocols, such as transarterial chemoembolization, radiofrequency wave, microwave, laser and cryogen, HIFU is featured with the distinctive advantages including non-invasive operation, small focus, non-radioactive and no damage to normal tissues in the acoustic-propagating path. Especially,

HIFU has been extensively applied clinically to treat several kinds of primary solid tumors and even metastatic cancer.[12-16] Abundant studies have shown that HIFU ablation is safe, effective and feasible.[17, 18] However, the efficiency of HIFU coagulation of deep-seated, larger volume and abundant blood-supplied tissues such as HCC is low due to the ultrasound energy attenuation and energy reduction in the areas that are adjacent to high-speed blood flow, which often needs higher ultrasound power and longer operation duration. However, the simple increase of ultrasound energy and operation time will cause undesired heating in intervening tissues and lead to unknown adverse events to normal tissue.

Fortunately, recent studies have proved that the HIFU-therapeutic efficiency can be synergistically enhanced by gas-filled microbubble ultrasound contrast agents (UCA).[19, 20] The main mechanism is based on the cavitation effect of HIFU. The particle size of microbubbles, however, is about several micrometers, thus blood-circulation time is limited, as well as the difficulty to penetrate tumor blood vessels and enter the tumor tissue.[21] Meanwhile, the nanosized bubbles only have very limited contrast-enhanced ultrasound imaging and HIFU-enhancing capability due to substantial decreased nonlinear backscattering with the reduction of particle size. In addition, microbubbles' shell is required to be modified with appropriate ligands that have homologous affinity and specificity to bind and cause retention of microbubble on the target tissue in the physiologic circulation conditions. Unfortunately, at present, this strategy is mainly adopted in pre-clinical studies due to inefficient targeted combination, hemodynamic and unwanted immune response.[22] It is urgent to solve HIFU targeting action of synergistic agents in the tumor area and minimize the particle size yet retain their contrast imaging and HIFU-enhancing performance.

Recently, various nanosystems such as mesoporous silicon nanoparticles,[23-30] magnetic nanoparticles,[31, 32] carbon nanotube,[33] poly (lactic-co-glycolic acid)(PLGA)[34] have shown excellent performances as either the ultrasound contrast agents or ultrasound synergistic agents for tumor diagnostic imaging and therapy. In addition, these nanosystems have been extensively explored in drug delivery, tissue engineering, multi-modality imaging and tumor-synergistic therapy.[35-43] Compared with traditional microbubbles, these nanoparticles show smaller size,

longer blood-circulation time, more stability and easier to be modified. It is noted that our group recently successfully developed organic PLGA nanocapsules for drug delivery, diagnostic imaging and enhanced HIFU surgery.[44-46] Herein, we further explored superparamagnetic Fe_3O_4-integratated PLGA capsules as the multifunctional nanosystems for multi-modality imaging-guided HIFU HCC cancer surgery, which were further used to deliver phase-changing agents to enhance HIFU-therapeutic efficiency. Different from traditional nanosystems to enhance HIFU-therapeutic efficiency, this work for the first time introduces transarterial chemoembolization to enhance the efficiency of nanoparticle-based synergistic HIFU cancer surgery. The combination of these two surgical strategies exhibits two distinctive mutual promotion effects. On one hand, the transarterial chemoembolization assisted by Lipiodol can substantially retain the synergistic agents within tumor tissues for subsequent HIFU cancer surgery. On the other hand, the second HIFU-irradiation step can further improve the efficiency of transarterial chemoembolization. Therefore, this research provides the first demonstration that the combination of transarterial chemoembolization and HIFU cancer surgery can bring with high tumor-surgical effect assisted by nano-biotechnology.

2. Materials and methods

2.1 Synthesis of multifunctional Fe_3O_4-PFH/PLGA nanocapsules

Multifunctional Fe_3O_4-PFH/PLGA nanocapsules integrating with superparamagnetic Fe_3O_4 nanoparticles and perfluorohexane (PFH) were prepared by a facile double-emulsion process. At first, 200 μL solution of oleic acid-capped Fe_3O_4 nanoparticles (25 mg/mL, size 10 nm, Ocean, USA) were added to 2 mL of CH_3Cl dissolving 100 mg of PLGA (50:50, MW = 12,000, Daigang, China). The mixture was emulsified using an ultrasonic probe (SONICS & MATERALS Inc; USA) at 130 W for 40 s after adding 100 μL of PFH (ABCR GmbH & Co. Germany). Then, the above emulsified solution was poured into 10 mL of poly (vinyl alcohol) (PVA, MW = 25,000, Sigma) solution (5%w/v) and homogenized (FJ300-SH, Shanghai, China) within 5 min for the second emulsion. The final emulsion was mixed with 10 mL of isopropanol (5%M/V, Chongqing Chuandong, China) and then mechanically agitated for 2 h to extract

CH_3Cl. Subsequently, the solution was centrifuged at 5000 rpm for 3 min, the supernatant was discarded, and the precipitate was rinsed by deionized water. The process of centrifugation was repeated for three times. Finally, the prepared Fe_3O_4-PFH/PLGA nanocapsules were stored under seal at 4℃ for further use. Fe_3O_4/PLGA, PFH/PLGA and pure PLGA nanocapsules were prepared by the similar procedure without the addition of PFH, OA-Fe_3O_4 nanoparticles solution and replaced with the same volume of deionized water. To further endow the nanocapsules with fluorescence-imaging capabilities, a typical red fluorescence dye DiI was introduced into the organic phase during the synthetic process. The encapsulation efficiency of PFH depended on the PFH amount used in the preparation process and the actual amount loaded into PLGA nanocapsules. Adopting small amount of PFH during the double-emulsion process would achieve high encapsulation efficiency. To achieve this goal, a small amount of PFH (100 μL) were added in the preparation process of PLGA nanocapsules. The quantitative encapsulation efficiency was difficult to be tested. Theoretically, PFH could almost completely encapsulate into PLGA nanocapsules due to the hydrophobic-hydrophobic interaction during double-emulsion process when the small amount of PFH was adopted, but it might have deviations during the preparation process.

2.2 Characterization of multifunctional Fe_3O_4-PFH/PLGA nanocapsules

The size distribution and the morphological observation were conducted by an inverted fluorescence microscope (Olympus IX51, Japan) and scanning electron microscope (SEM, Hitachi, S-3400N, Japan). The structure of Fe_3O_4-PFH/PLGA was analyzed using a transmission electron microscopy (TEM, Hitachi H-7600, Japan) at an accelerating voltage of 80 kV. Briefly, the samples were placed on a carbon-coated copper grid and stained with 3% (w/v) uranyl acetate for TEM viewing. A laser particle-size analyzer system (Zeta sizer3000HS; Malvern, UK) was used to acquire the mean particle size and Zeta potential of multifunctional nanocapsules.

2.3 Assessing the encapsulation efficiency of Fe_3O_4 nanoparticles in the Fe_3O_4-PFH/PLGA nanocapsules

Fe_3O_4 encapsulation efficiency in Fe_3O_4-PFH/PLGA nanocapsules was assessed by atomic absorption spectrometry. Briefly, 10 mg of lyophilized Fe_3O_4-PFH/PLGA nanocapsules was dissolved in 1 mL of dimethylsulfoxide. Then, 1 mL of 36 % HCl was added to decompose the Fe_3O_4, the free Fe ion was obtained, and the solution was diluted to a volume of 10 mL using 1 % HCl. The concentration of Fe_3O_4 in the solution was obtained from atomic absorption spectrometry (Hitachi model Z-5000, Hitachi Ltd, Tokyo, Japan). The encapsulation efficiency of Fe_3O_4 was calculated using the following equation: encapsulation efficiency of the Fe_3O_4 (%) = (the mass of Fe_3O_4 in the sample) / (the total mass of added Fe_3O_4) × 100 %.

2.4 *In vitro* phase transformation and ultrasound imaging of Fe_3O_4-PFH/PLGA nanocapsules

All *in vitro* ultrasound-imaging experiments were carried out on 2% agarose gel with columnar wells. The phase transformation of Fe_3O_4-PFH/PLGA nanocapsules was firstly operated on a DB-H model digital microscope thermostatic plate. About 50 μL of diluted Fe_3O_4-PFH/PLGA nanocapsules were extracted and dropped onto the microscope slide, and then the thermostatic plate was continuously heated from room temperature to 90 ℃ and observed under the optical microscope. The phase-changing temperature of nanocapsules was recorded. Correspondingly, an Eppendorf tube (5 mL in volume) filled with Fe_3O_4-PFH/PLGA nanocapsules was heated in thermostatic water bath according to the previous phase-transition temperature of the nanocapsules. Then, the samples were immediately scanned in B and contrast modes by an ultrasonic-diagnostic instrument. The samples of Fe_3O_4/PLGA, PLGA and PBS under the same condition was heated and scanned as well, and the ultrasonography at room temperature was acquired as the contrast. Furthermore, ultrasound-triggered evaporation of nanocapsule by HIFU (120W 5s) and low intensity focus ultrasound (LIFU, 8W 30s) irradiation was conducted, and the ultrasound image before and post exposure was observed.

2.5 *In vitro* MRI imaging

Fe_3O_4-PFH/PLGA nanocapsules were prepared at the concentrations of OA-Fe_3O_4 nanoparticles of 0, 20, 40, 60, 80, 100, 120, 140 μg/mL, which were imaged on 2% gel phantom

by clinical MRI equipment (Philips Achieva 3.0T TX MR Scanner, Philips Medical Systems, Netherlands). T_2-weighted images were acquired using the following parameters: fast field echo (FFE), TR = 3.2s, and TE = 80 ms, Flip = 90 °, FOV = 180 mm, slice thickness = 3.0 mm. The MRI signal intensity (SI) within the region of interest (ROI) was further measured.

2.6 *In vitro* photoacoustic (PA) imaging

To evaluate the PA imaging capability of Fe_3O_4-PFH/PLGA nanocapsules, a small animal PA imaging equipment (Vevo Laser, Canada) was used. This apparatus equips with a laser emission probe (the wavelength of the laser: between 680 - 950nm, excitation depth: about 1 cm), a diagnostic US probe and a computer processing system. The experiment was carried out using a gel mold (size: about 2 cm × 1 cm × 1 cm) with a hole of 1 cm in depth and 1 mm in diameter. 200 μL of Fe_3O_4-PFH/PLGA nanocapsules (Fe concentration = 300 μg/mL) were injected into the hole. Fe_3O_4/PLGA nanocapsules at the same concentration of Fe_3O_4-PFH/PLGA and pure PLGA nanocapsules with the same parameter were used and tested for comparison.

2.7 *Ex vivo* HIFU ablation against degassed bovine liver

Ex vivo HIFU ablation assay against degassed bovine liver was conducted against five groups: group I (normal saline), group II (pure PLGA), group III (Fe_3O_4/PLGA), group IV (PFH/PLGA), and group V (Fe_3O_4-PFH/PLGA). Typically, fresh bovine liver tissue (within 8 h after slaughter), 10cm×8cm×6cm in size, were immersed in deionized water at room temperature for 30 min. After being degassed, the bovine livers were placed and immersed in the container immersed filled with degassed water. Normal saline, pure PLGA, Fe_3O_4/PLGA, PFH/PLGA, Fe_3O_4-PFH/PLGA nanocapsules suspension in 1× PBS (200 μL,) were directly injected into the bovine liver using a syringe (1 mL in volume), and the injection site was real-time monitored by a diagnostic US unit. Immediately after the agent was injected, HIFU was acted on the injection site. The HIFU ablation parameters were described as follows: acoustic power = 120 W, 150 W, 180 W and exposure duration = 3 s. After HIFU ablation, the volume of coagulated tissues in the degassed bovine liver was calculated by the following equation: $V = \pi/6 \times L \times W \times D$ (L: length, W: width, D: depth). Gray-scale changes of the five groups after HIFU irradiation were acquired

on the diagnostic ultrasound images within the focus, which was used during the ablation procedure to identify and monitor the efficiency of HIFU treatment.

2.8 *In vivo* experiments

2.8.1 Animal xenograft of rabbits

All animal experiments were approved by Chongqing Medical University animal ethics committee. Tumor-bearing rabbits with a VX2 tumor (VX2 squamous carcinoma cell line; Funabashi Farm Co, Kyoto, Japan) in the liver were obtained from the laboratory of Ultrasound Engineering Institute of Chongqing Medical University. New Zealand white rabbits weighing 2.0-2.5 kg and between 2 and 3 months-old were purchased from and bred in the Animal Center of Chongqing Medical University under standard conditions according to the Institute's environmental guidelines.

Under sterile conditions, the fish-meat-like tumor tissue was excised from the tumor-bearing rabbit, washed with normal saline, and then subdivided into small tissue pieces about 1 mm^3, which was soaked in 20 mL of Hanks' balanced salt solution for further using. One day before modeling, the abdomens of rabbits were depilated with 8% Na_2S solution. Rabbits were anesthetized by injecting of 3% pentobarbital solution (1 mL/kg) into the ear vein, and then fixed in prone position and routinely disinfected. A median incision was made below the xiphoid to expose the middle lobe of liver, where a cavity about 5 mm in deep was made using ophthalmological forceps, then one tissue piece was implanted into the hole. After bleeding was stopped with gauze oppression, the abdominal wall was sutured. Skin incision was sterilized with povidone iodine, and 800,000 units penicillin was intramuscular injected for three consecutive days to prevent infection.

2.8.2 *In vivo* MRI imaging

Twenty-one days after VX2 tumor inoculation in the liver, 16 rabbits with detectable liver cancer were divided into four groups: group I (Fe_3O_4-PFH/PLGA), group II (Fe_3O_4/PLGA), group III (PLGA) and group IV (normal saline). *In vivo* T_2-weighted MRI imaging was carried

out after animals were anaesthetized before and at 1 min after intravenous injections (1 mL/kg) of Fe_3O_4-PFH/PLGA nanocapsules (937 μgFe/mL), Fe_3O_4/PLGA(946 μgFe/mL), PLGA (without Fe_3O_4) and normal saline. To acquire T_2-weighted images, the following parameters were used: TR = 680 ms, TE = 60 ms, Flip = 90 °, FOV = 60 mm, and slice thickness = 1 mm.

2.8.3 *In vivo* transcatheter arterial injection of Fe_3O_4-PFH/PLGA and Lipiodol emulsion simultaneously

Three weeks after implantation of VX2 tumors, twenty VX2 tumor-bearing rabbits were divided into 4 groups: group I (normal saline), group II (Lipiodol), group III (Fe_3O_4-PFH/PLGA), and group IV (Lipiodol combined with Fe_3O_4-PFH/PLGA). Transcatheter arterial embolization process was carried out using flat-panel digital subtraction angiography equipment (Philips Allura Xper FD20, Netherlands). The bilateral groin skin was depilated using 8%Na_2S solution and fasted eight hours before the operation. The rabbits were fixed on the operating table in the prone position. Regular skin disinfection and the drapes spread were executed. Then, the right groin shin was cut open and femoral artery was isolated carefully, and the artery proximal was clipped by a vascular clamp. An incision was made at the anterior wall of the femoral artery by ophthalmic scissors, and then a microcatheter (Terumo, Japan) was inserted into the right femoral artery. Under fluoroscopic guidance, the catheter tip was selectively located in the proper hepatic artery. Hepatic artery angiography was executed to display the blood-vessel distribution of VX2 Hepatic carcinoma. The agentia of each group was injected through the microcatheter. One hour later, the rabbit liver was scanned by spiral CT (LightSpeed Ulra16, Philips, Netherlands) to observe the Lipiodol emulsion distribution inside tumor.

2.8.4 *In vivo* HIFU ablation

Model-JC200 HIFU tumor ablation equipment (Chongqing Haifu Technology, Chongqing, China) was used in this study. This apparatus consists of US therapy transducers with a US generator, a real-time diagnostic US device, a six-direction movement system, computer units for automated control, a treatment bed and a degassed water circulation unit. A 12-cm diameter PZT-4 piezoceramic transducer was employed to produce therapeutic US energy. The frequency

of the transducers was 0.8 MHz with various focal lengths ranging from 135-155mm. The focused US transducer emits high intensity ultrasound to target and destroy tissue of interest. The diagnostic transducer was located in the center of the therapeutic transducer to guide and monitor the therapeutic process in real-time. Degassed water was used as the medium in these ultrasound therapies.

One day after twenty VX2 Hepatic carcinoma rabbits treated by TAE operation, HIFU ablation was implemented. The abdominal hairs of rabbits had been carefully depilated with 8% Na_2S before HIFU ablation. After anesthetizing with 3%pentobarbital (1 mL/kg), the rabbits were placed on the HIFU treatment bed in the prone position, and the depilated area of the epigastrium was completely immersed in the degassed water. Tumor was orientated and measured by integrated diagnostic ultrasound imaging before ablation. The groups were sorted with above TAE operation: HIFU combined with saline (I, n =5), HIFU combined with Lipiodol (II, n=5), HIFU combined with Fe_3O_4-PFH/ PLGA nanocapsules (III, n = 5) and HIFU combined with Lipiodol plus Fe_3O_4-PFH /PLGA (IV, n = 5). “Ablated-dot” mode was adopted indicating that each tumor was destroyed in one single exposure. In all four groups, HIFU ablation parameters were kept the same at the acoustic power of 180 W and exposure duration of 3 s. During HIFU treatment, the ablation effects were assessed using diagnostic-ultrasound images in real-time. Coagulated tissues by HIFU ablation appeared hyperechogenic on ultrasound image. Pre-and post-ablation, gray scale of the targeted areas was automatically compared using Gray Val 1.0 software affiliated to HIFU equipment. Seventy-two hours after HIFU ablation, the animals were euthanized and the VX2 tumors were harvested for macroscopic and microscopic examinations.

2.8.5 Detection of iron oxide and Lipiodol components within tumor tissue

The detection of iron oxide nanoparticles and Lipiodol was designed to observe the nanocapsule distribution within tumor tissues. Day 3 after transcatheter arterial embolization (TAE), the rabbits were euthanized by a lethal dose of pentobarbital and tumors were harvested. Two tumor tissues were selected of every group and made into frozen section. Then, Lipiodol

was detected by Oil Red O staining, and iron oxide nanoparticles were expressed by Prussian blue staining.

2.8.6 Histopathological analysis

At day 3 after the TAE combined with HIFU ablation, tumor tissues for histological analysis were harvested from all four groups' rabbits. One cm^3 tissue containing the ablated zone and the surrounding zone from each tumor was excised, fixed in 4% Paraformaldehyde solution, routinely processed and paraffin embedded stained with hematoxylin and eosin (HE) for pathological examination. Immunohistochemical examination on targeted tissue was also performed to acquire information on proliferation of these tissues using proliferating cell nuclear antigen (PCNA, Boster, China). PCNA expresses in the cell nucleus. Apoptosis express was also evaluated on these tissue sections using TdT-mediated dUTP nickend labeling (TUNEL, Roche, Switzerland) assay. A homogeneous brown color of the nucleus suggests that cells are PCNA or TUNEL positive. The positive cell count was semi-quantitatively obtained by counting the number of cells stained positively from at least 5 random selected high-magnification (×400 magnifications) fields by blind observers. The proliferating index (PI) and apoptotic index (AI) expressed as the ratio of positively stained tumor cells to all cells were determined by the same way as mentioned above.

2.9 Statistical analysis

All results were mentioned as mean values ± standard deviation (SD). Statistical differences for multiple groups were analyzed using a one way ANOVA and individual groups were compared using Student's t-test. $P < 0.05$ was regarded as a significant difference.

3. Results and discussion

3.1 Design of multifunctional Fe_3O_4-PFH/PLGA nanocapsules for transarterial chemoembolization-enhanced HIFU-synergistic cancer surgery

In this work, we successfully developed a biocompatible multifunctional nanosystem with phase-changing features for transarterial chemoembolization-enhanced HIFU-synergistic cancer surgery (**Scheme 1**). PLGA nanocapsules were preferably chosen because it is a FDA-approved biomaterial on account of their high stability, biodegradability and biocompatibility, which ensures acoustic properties and prolonged circulation time, and high safety for *in vivo* applications and further clinical translations.[34] Magnetic Fe_3O_4 were then integrated into the shell of PLGA nanocapsules because they can act as contrast agents for T_2-weighted magnetic resonance imaging (MRI).[47] In addition, recent research has shown that magnetic Fe_3O_4 nanoparticles can also be used as the contrast agents for photoacoustic (PA) imaging.[48-50] In addition, superparamagnetic Fe_3O_4 nanoparticles can sensitize the tumor to the effects of hyperthermia.[31] Furthermore, hydrophobic perfluorohexane (PFH) was introduced into the core of Fe_3O_4/PLGA nanocapsules because of its desirable boiling point of 56 ℃, which can be vaporized by the thermal effect of HIFU. Such a phase-changing and bubble-generation procedure is expected to substantially improve the performances of ultrasound imaging and HIFU cancer surgery.[51] A typical double emulsion process was employed to concurrently embed Fe_3O_4 nanoparticles into the shell of PLGA and liquid PFH into the core of PLGA nanocapsules.

The Fe_3O_4-PFH/PLGA nanocapsules were then accumulated into liver cancer by means of passive targeting *via* transarterial injection assisted by Lipiodal emulsion, a typical tumor blood vessel-blocking agent for transarterial chemoembolization (**Scheme 1**). The elaborate combination of Fe_3O_4-PFH/PLGA and Lipiodal can transiently block blood flow and prolong/increase the accumulation of composite nanocapsules just within the tumor area. The subsequent PFH bubble generation from Fe_3O_4-PFH/PLGA *via* HIFU irradiation further enhances the cavitation effect and simultaneously promotes micro-vessel occlusion of tumor. In addition, the integration of Fe_3O_4 nanoparticles could bring with the multi-modality imaging capability, which could be used for precise diagnostic-imaging, imaging guidance and potential hyperthermia application. Therefore, the multifunctional Fe_3O_4-PFH/PLGA nanocapsules combined with Lipiodol were developed to be capable of: 1) exploiting hepatic artery (HA) catheter injection targeting to tumors, 2) substantially increased accumulation and retention

within tumor tissues, 3) MR/US/PA multi-modality imagings and guidances and 4) synergistic/efficient cancer surgery involving HIFU, transarterial chemoembolization and acoustic droplet vaporization.

3.2 Synthesis and characterization of Fe_3O_4-PFH/PLGA nanocapsules

Multifunctional phase-changing Fe_3O_4-PFH/PLGA composite nanocapsules were synthesized by a simple yet versatile double emulsion process. Oleic acid-capped hydrophobic Fe_3O_4 nanoparticle and hydrophobic PFH molecules could be simultaneously encapsulated into PLGA nanocapsules *via* this facile process (see experimental section). The as-synthesized Fe_3O_4-PFH/PLGA nanocapsules exhibit uniform spherical morphology and high dispersity (**Figure 1a**). The Dil dye was further encapsulated into Fe_3O_4-PFH/PLGA nanocapsules to show their capability of loading guest molecules, such as anticancer drugs (**Figure 1b**). Scanning electron microscope (SEM) image of Fe_3O_4-PFH/PLGA nanocapsules directly shows the spherical morphology and smooth surface of nanocapsules (**Figure 1c**), indicating the successful encapsulation of Fe_3O_4 nanoparticles into the shell of PLGA. Transmission electron microscope (TEM) image of single Fe_3O_4-PFH/PLGA nanocapsule exhibits the strong contrast difference (**Figure 1d**), and the spherical Fe_3O_4 nanoparticles could be clearly distinguished in the composite nanocapsules. The mean diameter and Zeta potential of Fe_3O_4-PFH/PLGA nanocapsules were determined to be 561.9 ± 207.2 nm and -29.3 mV, respectively, which were required by dynamic light scattering (DLS, **Figure 1e**) and electrophoretic light scattering (ELS, **Figure 2f**) measurements. The amount of Fe_3O_4 nanoparticles encapsulated in the nanocapsules measured by atomic absorption spectrometry method was 937.5 ± 86.3μg/mL, and encapsulation efficiency of Fe_3O_4 was 46.9wt%.

3.3 *In vitro* phase transformation and ultrasound-imaging capabilities of Fe_3O_4-PFH/PLGA nanocapsules

The as-synthesized Fe_3O_4-PFH/PLGA nanocapsules are featured with unique phase-changing capability for ultrasound imaging and therapy. In this regard, this nanosystem can realize “small-to-big” protocol to overcome the drawbacks of traditional microbubbles. The

particle size of Fe_3O_4-PFH/PLGA nanocapsules is small enough to enter and accumulate into tumor tissue during the transportation within blood vessel, which can be vaporized to generate bubbles with large particle size by the thermal effect of HIFU. The subsequent post-generated bubbles can substantially change the acoustic microenvironment of tumor tissues and enhance the HIFU-therapeutic efficiency accordingly.

The phase-transformation phenomenon of Fe_3O_4-PFH/PLGA nanocapsules was directly observed by optical microscopy at different temperatures (**Figure 2a**). The liquid PFH core of Fe_3O_4-PFH/PLGA nanocapsules could be vaporized into gas and generate microbubbles subsequently. No microbubbles were found in Fe_3O_4-PFH/PLGA nanocapsules at 56 ℃ (**Figure 2a$_1$**), indicating no phase transformation occurred due to the low temperature. Microbubbles generated when the temperature rose to 64 ℃ (**Figure 2a$_2$**), and bubble volume and amount increased accompanying with the increase of temperature (**Figure 2a$_3$**). When the temperature reached 80 ℃, almost all particles were found to be converted into large amounts of bubbles (**Figure 2a$_4$**), and some microbubbles began to collapse. At the higher temperature of 90 ℃, only a few very large bubbles could be observed (**Figure 2a$_5$**). Interestingly, the corresponding *in vitro* enhancement of ultrasound imaging was consistent with the phase transformation observed under optical microscopy (**Figure 2b**). When the temperature was above 70 ℃, a significant enhancement of acoustic responses was found in Fe_3O_4-PFH/PLGA and PFH/PLGA nanocapsules under the contrast model of ultrasound, the mode of which is only sensitive to bubbles. Comparatively, no contrast enhancement was observed in PBS with the increased temperature. This result provides the strong evidence that Fe_3O_4-PFH/PLGA nanocapsules could performance the phase-changing capability to generate PFH bubbles and substantially response to ultrasound subsequently.

Such a phase-changing phenomenon of Fe_3O_4-PFH/PLGA nanocapsules could also be triggered by HIFU. As shown in **Figure 2c**, the grey intensity and area of Fe_3O_4-PFH/PLGA nanocapsules displayed the most obvious changes among three samples at the condition of irradiation power of 150 W and irradiation duration of 5s after HIFU irradiation. The thermal

effect of HIFU is responsible for such a phase-changing procedure where the PFH core of Fe_3O_4-PFH/PLGA nanocapsules could be vaporized by HIFU irradiation. Interestingly, phase changing of Fe_3O_4-PFH/PLGA nanocapsules could also be triggered by low-intensity focused ultrasound (LIFU, **Figure 2d**), which is possibly attributed to the cavitation effect induced by LIFU irradiation to cause the phase changing of PFH in the core. Therefore, the *in vitro* HIFU and LIFU irradiation results demonstrated that the as-synthesized Fe_3O_4-PFH/PLGA nanocapsules could act as a phase-change synergistic agent for enhancing HIFU ablation efficiency.

3.4 Fe_3O_4-PFH/PLGA nanocapsules as the contrast agents for multi-modality diagnostic MR and PA imaging

The process of HIFU surgery typically requires external diagnostic-imaging guidance to find out the lesion tissues. Ultrasound and MR imagings are currently used in clinic for HIFU guidance. To further improve the imaging resolution and precision, superparamagnetic Fe_3O_4 nanoparticles were integrated with PLGA nanocapsules, which acted as the contrast agents for T_2-weighted MR imaging. As revealed in the MR phantom images (**Figure 3a**), Fe_3O_4-PFH /PLGA nanocapsules negatively enhanced the T_2-weighted MR images. The MRI signal intensity decreased in accordance to the increase of iron concentrations (**Figure 3b**), demonstrating that Fe_3O_4-PFH/PLGA nanocapsules have produced the MR contrast on transverse photon relaxation time-weighted sequence. This could account for the dipolar interaction of the magnetic moment of the superparamagnetic nanocapsules and protons in water, which further strongly demonstrated that the superparamagnetic Fe_3O_4-PFH/PLGA nanocapsules could generate the negative contrast-enhanced effect for T_2-weighted MR imaging.

Importantly, the intravenous administration of either Fe_3O_4-PFH/PLGA or Fe_3O_4/PLGA nanocapsules into rabbit bearing VX2 tumor in liver could produce substantial negative T_2 signal in MR imaging (**Figure 3c and d**), demonstrating the high efficiency of Fe_3O_4-PFH/PLGA for T_2-weighted MR imaging and further potential for HIFU guidance. Comparatively, the administration of pure PLGA nanocapsules could not cause such a negative effect in MR images,

further indicating the versatility and functionality of the integration of superparamagnetic Fe_3O_4 nanoparticles into PLGA nanocapsules.

It is noted that the integrated superparamagnetic Fe_3O_4 nanoparticles could also act as the contrast agents for PA imaging. The PA-imaging capability of Fe_3O_4-PFH/PLGA nanocapsules was assessed on a gel phantom at room temperature *in vitro*. The contrast-enhanced capability of Fe_3O_4-PFH/PLGA, Fe_3O_4/PLGA and pure PLGA nanocapsules (without integrated OA-Fe_3O_4 nanoparticles) were compared for PA imaging. As shown in **Figure 4a**, a distinct PA-signal peak appeared at the wavelength of λ = 695 nm in Fe_3O_4-PFH/PLGA and Fe_3O_4/PLGA samples with signal intensity up to 2.0 and 2.62, respectively, as irradiated by near infrared laser at wavelength between 680-950nm. Comparatively, the PA-signal intensity of pure PLGA nanocapsules was extremely low. In addition, the spectrum curve of pure PLGA was irregular.

It is also noted that the PA signal of Fe_3O_4-PFH/PLGA and Fe_3O_4/PLGA nanocapsules revealed no obvious attenuation accompanying with extended laser-exposure duration irradiated by laser at the wavelength of 695 nm (**Figure 4b**). Moreover, the PA intensity of the nanocapsules integrated with Fe_3O_4 nanoparticles was nearly five folds compared to pure PLGA nanocapsules. The signal-intensity difference between Fe_3O_4-PFH/PLGA and Fe_3O_4/PLGA might be related to the distribution-status difference of Fe_3O_4 nanoparticles within PLGA shell. The PA-imaging assay also suggested that there were minimal effects on the integration of Fe_3O_4 nanoparticles within PLGA shells to maintain their PA-imaging capability. Combined with excellent contrast-enhanced capability of Fe_3O_4-PFH/PLGA nanocapsules for ultrasound and MR imaging, this *in vitro* investigation suggested that Fe_3O_4-PFH /PLGA nanocapsules could act as the potential multi-modality contrast agents for ultrasound, PA and MR tri-modal imaging.

3.5 *Ex vivo* synergistic effect of Fe_3O_4-PFH/PLGA composite nanocapsules for HIFU ablation

Based on the intriguing performance of phase transformation of Fe_3O_4-PFH/PLGA composite nanocapsules, their synergistic effect on HIFU ablation was systematically

investigated employing fresh degassed bovine liver as the *ex vivo* tissue model. The degas procedure was pre-conducted to avoid the influence of possible air bubbles in the tissues. After the direct injection of different agents including PBS, pure PLGA, Fe_3O_4/PLGA, PFH/PLGA and Fe_3O_4-PFH /PLGA, HIFU was directly focused on the injection site by the external guidance of ultrasound imaging. After the irradiation, the bovine liver was dissected to calculate the coagulation volume.

As shown in **Figure 5a**, the HIFU ablation volume increased gradually as the increase of adopted ultrasound power (120 W, 150 W and 180 W). Especially, Fe_3O_4-PFH/PLGA composite nanocapsules with phase-changing capability could induce substantially larger tissue-ablation volume compared to PFH/PLGA, Fe_3O_4/PLGA, pure PLGA and PBS as the control ($P < 0.05$, **Figure 5b**). Theoretically, during HIFU treatment, the temperature in focal area can reach up to 65 - 100 ℃ within 0.5 - 1.0 s. However, ultrasound energy attenuates in deep tissue, which decreases the energy deposition in target region and affects the efficiency of HIFU surgery. The intervention of micro- or nanocapsules could change the acoustic environment of tissues, and thus increase the HIFU energy deposition to improve the therapeutic efficiency. The addition of Fe_3O_4 nanocapsules induced obvious signal enhancement, implying that Fe_3O_4 nanoparticles could synergistically improve the ablation efficiency of HIFU at lower power and shorter exposure duration. Two main factors may be related to the effect of Fe_3O_4-PFH/PLGA better than PFH/PLGA: first, Fe_3O_4 nanoparticles as metal oxide adding in the composite nanocapsules could change the acoustic impedance; second, they may improve the heat-transferring rate in tissue. Fe_3O_4-PFH/PLGA exhibited higher efficiency than Fe_3O_4/PLGA regarding the tumor ablation, which was due to the phase-changing of PFH in the core, generated bubbles, increased cavitation effect and substantially changed tissue acoustic impedance.

3.6 *In vivo* transarterial chemoembolization to enhance nanocapsule-based HIFU synergistic cancer surgery

We for the first time used *in vivo* transarterial chemoembolization to substantially increase the accumulation and retention amount of Fe_3O_4-PFH/PLGA nanocapsules within tumor tissue *via* hepatic-artery injection coupled with Lipiodol emulsion. The high accumulation of Fe_3O_4-PFH/PLGA within the tumor tissue could substantially enhance the HIFU surgical efficiency. Meanwhile, the further HIFU synergistic therapy could improve the efficiency of traditional *in vivo* transarterial chemoembolization, which means that the typical HIFU ablation and transarterial chemoembolization could be combined to achieve high tumor-therapeutic outcome assisted by Fe_3O_4-PFH/PLGA nanocapsules.

The mixture of Fe_3O_4-PFH/PLGA nanocapsules and Lipiodol was initially injected through hepatic artery by a microcatheter, typically used in transarterial chemoembolization. As shown in **Figure 6a**, the rabbit VX2 hepatic carcinoma angiography revealed that the tumor area exhibited significant difference from the surrounding normal tissue because of the presence of rich tumor vessels. After being infused with Fe_3O_4-PFH/PLGA and Lipiodol emulsion *via* microcatheter, the flow velocity of VX2 tumor vessels slowed down and the Fe_3O_4-PFH/PLGA nanocapsules accumulated within the tumor area (**Figure 6b**). Interestingly, the normal liver tissue appeared as very little Lipiodol deposition. Moreover, the mixture emulsion was mainly distributed in the VX2 cancer area (**Figure 6c and d**). One hour after TAE operation, the CT imaging (**Figure 6e**) was consistent with the result of digital subtraction angiography (DSA) that Fe_3O_4-PFH/PLGA and Lipiodol emulsion were mainly accumulated within tumor tissue.

Transcatheter arterial embolization was initially proposed to treat HCC in 1974.[9] In fact, Lipiodol-based transarterial chemoembolization is generally recognized as the gold-standard therapy in intermediate or advanced HCC patients.[10] Lipiodol is featured with the characteristics of passive deposition in HCC blood vessels and subsequent blood-vessel blocking capability. The as-synthesized Fe_3O_4-PFH/PLGA nanocapsules had hydrophobic PLGA shell, which could uniformly mix with Lipiodol for easy injection by a microcatheter. The DSA results suggested that Lipiodol successfully carried Fe_3O_4-PFH/PLGA nanocapsules into the tumor, accumulated the nanocapsules within tumor tissues with high retention amount and blocked the blood vessels subsequently.

One day after the transarterial chemoembolization procedure and accumulation of Fe_3O_4-PFH/PLGA within tumor tissue at high amount, *in vivo* HIFU ablation was directly conducted on the tumor tissues. The HIFU synergistic enhancement and associated synergistic mechanism was systematically evaluated. The navigation of tumor and HIFU-ablation effect were observed under a real-time ultrasound-imaging unit of the HIFU-therapeutic system. Tumor was treated at the HIFU power of 180 W and exposure duration of 5 s. After HIFU exposure, the acoustic signals varied significantly by the administration of different agents (**Figure 7a and b**). The mixture of Fe_3O_4-PFH/PLGA and Lipiodol emulsion caused the most distinct ultrasound-signal enhancement, suggesting that such an agent could cause the highest synergistic effect for HIFU ablation. After three days, rabbits in each group were sacrificed and the tumor tissues were excised to calculate the ablation volumes. As shown in **Figure 7c and d**, the volume of coagulation necrosis was largest in the group of Fe_3O_4-PFH/PLGA combined with Lipiodol compared to other three groups with saline, Lipiodol and Fe_3O_4-PFH/PLGA under the same HIFU-irradiation condition. These *ex vivo* tumor-ablation results (**Figure 7c and d**) were consistent with *in vivo* ultrasound imaging outcomes (**Figure 7a and b**), which indicated that Fe_3O_4-PFH/PLGA nanocapsules combined with Lipiodol embolization could substantially improve the HIFU-ablation efficiency because the blood vessel-blocking effect of Lipiodol embolization could not only substantially increase the accumulation amount of Fe_3O_4-PFH/PLGA nanocapsules within tumor but also can restrict the nanocapsules within the tumor tissues to further maximize the HIFU synergistic efficiency (**Figure 7e**). The subsequent vaporization of PFH core and generation of PFH bubbles further enhance the HIFU-ablation efficiency.

It is well-known that the temperature in focus area can rise to 65-100 ℃ in 0.5 -1.0 s during HIFU surgery, which generates thermal and cavitation effect, acoustic streaming and shear stresses to induce coagulation necrosis.[44] The temperature of focus site is sufficient to induce the phase transformation of PFH core. Fe_3O_4-PFH /PLGA nanocapsules could generate microbubbles upon the HIFU irradiation under high-energy focused ultrasound beam. This procedure could change the acoustic environment of tumor tissues. In addition, the generated

microbubbles could enhance the cavitation effect and shear stresses caused by HIFU, and then increase the coagulation volume of HIFU ablation accordingly. It is noted that Lipiodol could also change tumor tissues acoustic situation.[51-54] In this regard, Lipiodol combined with microbubbles could transiently obstruct tumor microvessels, enhance the acoustic-energy deposition and decrease energy consumption to improve the HIFU-therapeutic efficiency because vessels around tumor could take the thermal energy away.[51 55-56]

To further validate the deposition of Fe_3O_4-PFH/PLGA nanocapsules and Lipiodol within tumor tissue, optical microscopic images of tumor-tissue slices after Prussian blue (**Figure 8a**) and oil red (**Figure 8b**) staining were obtained, which validated the presence of iron and Lipiodol in the nanocapsules, respectively. Comparatively, no blue and red staining was observed in the tumor tissues administered without Fe_3O_4 nanoparticles or Lipiodol. HE staining (**Figure 8c**) further demonstrated that HIFU ablation assisted by Lipiodol combined with Fe_3O_4-PFH/PLGA could cause the large-scale tumor necrosis compared with tumors receiving the administration of other agents.

For the evaluation of VX2 tumor-cell proliferation and apoptosis in the liver of rabbits after HIFU ablation, immunohistochemical staining with antibodies against proliferating cell nuclear antigen (PCNA) and TdT-mediated dUTP nickend labeling (TUNEL) assay was performed. The results showed that the proliferative index (PI) in the group of Lipiodol combined with Fe_3O_4-PFH/PLGA was significantly lower than those of any other groups ($p < 0.05$) (**Figure 9a and 10a**). Apoptotic cells showed brown staining in the nuclei. Similar to the proliferation assay, our results also exhibited that apoptotic cells were observed in all groups, and the apoptotic index (AI) for the tumor in the group of Lipiodol combined with Fe_3O_4-PFH/PLGA was significantly higher than those of the other groups ($p < 0.05$) (**Figure 9b and 10b**). The immunohistochemical examination further demonstrates the high efficiency of Lipiodol combined with Fe_3O_4-PFH/PLGA for synergistic HCC cancer surgery.

4. Conclusions

In summary, we have developed a facie and versatile nanoparticle (Fe_3O_4-PFH/PLGA)-based HIFU synergistic cancer surgery enhanced by transarterial chemoembolization for high-efficient HCC treatment, which was successfully demonstrated in VX2 liver-tumor xenograft in rabbits. Multifunctional Fe_3O_4-PFH/PLGA nanocapsules were elaborately designed and fabricated, which were further developed as the contrast agents for ultrasound, MR and PA tri-modality imagings and as the synergistic agents for enhanced HIFU ablation because of the integration of superparamagnetic Fe_3O_4 nanoparticles within the shell and phase-transformation performance of PFH inner core. Importantly, these multifunctional Fe_3O_4-PFH/PLGA nanocapsules were administrated *in vivo* by means of transarterial injection combined with Lipiodol, which could substantially accumulate the nanocapsules within tumor tissues and enhance the therapeutic efficiency against HCC tumors. In addition, the combination of transarterial chemoembolization with nanoparticle-enhanced HIFU surgery could efficiently enhance the HCC cancer-treatment outcome, initiating a new therapeutic protocol for cancer treatment. This work also provides a versatile approach for the accumulation enhancement of nanoparticle-based synergistic agents for HIFU cancer surgery by blocking the blood vessels *via* transarterial chemoembolization.

Acknowledgements

The authors greatly appreciate Dr. Liu Zuojin's assistance on the device of transarterial chemoembolization operation, Wang Qi and Yao Yuanzhi for their collaboration in HIFU technical support, Dr. Song Weixiang, Dr. Wu Wei for their assistance with MR imaging and Dr. Hao Lan for her assistance with PA imaging. This work was supported in part by Program for Innovation Team Building at Institutions of Higher Education in Chongqing (Grant No. KJTD201303) and the National Nature Science Foundation of China (Grant No. 81371578).

References

1. J. D. Yang and L. R. Roberts, *Nat Rev Gastroenterol Hepatol.*, 2010, **7**, 448-458.
2. Z. V. Fong and K. K. Tanabe, *Cancer*, 2014, **120**, 2824-2838.
3. S. Ni, L. Liu and Y. Shu, *J. Biomed. Res.*, 2012, **26**, 260-267.
4. N. N. Rahbari, A. Mehrabi, N. M. Mollberg, S. A. Müller, M. Koch, M. W. Büchler and J. Weitz, *Ann. Surg.*, 2011, **253**, 453-469
5. T. J. Vogl, R. Straub, K. Eichler, O. Sollner and M. G. Mack, *Radiology*, 2003, **230**, 450-458.
6. K. Mafune and Y. Tanaka, *Ann. Surg. Oncol.*, 2000, **7**, 609-616.
7. D. B. Johnson and S. Y. Nakada, *J. Endourol.*, 2003, **17**, 627-632.
8. S. N. Goldberg, *Radiology*, 1998, **209**, 371-379.
9. D. Doyon, A. Mouzon, A. M. Jourde, C. Regensberg and C. Frileux, *Annales de radiologie*, 1974, **17**, 593-603.
10. J. M. Idee and B. Guiu, *Crit Rev Oncol Hematol*, 2013, **88**, 530-549.
11. S. Wang, C. Yang, J. Zhang, X. R. Kong, H. Zhu, F. Wu and Z. Wang, *Hepatology*, 2014, **59**, 170-177.
12. F. Wu, *Ultrasound Med. Biol.*, 2004, **30**, 245-260.
13. F. Wu, *J. Urol.*, 2003, **170**, 2237-2240.
14. F. Wu, Z. B. Wang, W. Z. Chen, W. Wang, Y. Z. Gui, M. Zhang, G. Q. Zheng, Y. J. Zhou, G. L. Xu, M. Li, C. W. Zhang, H. Y. Ye and R. Feng, *Ultrason. Sonochem.*, 2004, **11**, 149-154.
15. G. Vallancien, M. Harouni, B. Guillonneau, B. Veillon and J. Bougaran, *Urology*, 1996, **47**, 204-207.
16. S. Thuroff, *J. Endourol.*, 2003, **17**, 673-677.
17. S. Thuroff and C. Chaussy, *Mol. Urol.*, 2000, **4**, 183-187.
18. E. A. Stewart, *Am. J. Obstet. Gynecol.*, 2003, **189**, 48-54.
19. D. J. Chung, S. H. Cho, J. M. Lee and S. T. Hahn, *Eur. J. Radiol.*, 2012, **81**, 519-523.

20. W. He, W. Wang, P. Zhou, Y. X. Wang, P. Zhou, R. Z. Li, J. S. Wang and A. T. Ahuja, *Cardiovasc. Intervent. Radiol.*, 2011, **34**, 1050-1057.
21. X. Zhang, Y. Zheng, Z. Wang, S. Huang, Y. Chen, W. Jiang, H. Zhang, M. Ding, Q. Li, X. Xiao, X. Luo and H. Qi, *Biomaterials*, 2014, **35**, 5148-5161.
22. S. Unnikrishnan and A. L. Klibanov, *AJR Am J Roentgenol*, 2012, **199**, 292-299.
23. X. Wang, H. Chen, Y. Zheng, M. Ma, Y. Chen, K. Zhang, D. Zeng and J. Shi, *Biomaterials*, 2013, **34**, 2057-2068.
24. Y. Chen, H. R. Chen and J. L. Shi, *Acc. Chem. Res.*, 2014, **47**, 125-137.
25. Y. Chen, H. R. Chen, Y. Sun, Y. Y. Zheng, D. P. Zeng, F. Q. Li, S. J. Zhang, X. Wang, K. Zhang, M. Ma, Q. J. He, L. L. Zhang and J. L. Shi, *Angew. Chem.-Int. Edit.*, 2011, **50**, 12505-12509.
26. Y. Chen, H. Chen and J. Shi, *Adv. Healthc. Mater.*, 2015, **4**, 158-165.
27. H. P. Martinez, Y. Kono, S. L. Blair, S. Sandoval, J. Wang-Rodriguez, R. F. Mattrey, A. C. Kummel and W. C. Trogler, *Medchemcomm*, 2010, **1**, 266-270.
28. Y. Chen, H. R. Chen and J. L. Shi, *Adv. Mater.*, 2013, **25**, 3144-3176.
29. Y. Chen, Q. Yin, X. F. Ji, S. J. Zhang, H. R. Chen, Y. Y. Zheng, Y. Sun, H. Y. Qu, Z. Wang, Y. P. Li, X. Wang, K. Zhang, L. L. Zhang and J. L. Shi, *Biomaterials*, 2012, **33**, 7126-7137.
30. J. L. Shi, Y. Chen and H. R. Chen, *J. Inorg. Mater.*, 2013, **28**, 1-11.
31. S. K. J. Paul Moroz, Jillean Winter,Bruce N. Gray, *J. Surg. Oncology*, 2001. **78**, 22-29.
32. M. A. Malvindi, A. Greco, F. Conversano, A. Figuerola, M. Corti, M. Bonora, A. Lascialfari, H. A. Doumari, M. Moscardini, R. Cingolani, G. Gigli, S. Casciaro, T. Pellegrino and A. Ragusa, *Adv. Funct. Mater.*, 2011, **21**, 2548-2555.
33. R. Klingeler, S. Hampel and B. Buchner, *Int J Hyperthermia*, 2008, **24**, 496-505.
34. J. Panyam and V. Labhasetwar, *Adv. Drug Deliv. Rev.*, 2003, **55**, 329-347.
35. R. L. Manthe, S. P. Foy, N. Krishnamurthy, B. Sharma and V. Labhasetwar, *Mol. Pharm.*, 2010, **7**, 1880-1898.
36. N. Rapoport, Z. Gao and A. Kennedy, *J. Natl. Cancer I.*, 2007, **99**, 1095-1106.

37. K. K. Coti, M. E. Belowich, M. Liong, M. W. Ambrogio, Y. A. Lau, H. A. Khatib, J. I. Zink, N. M. Khashab and J. F. Stoddart, *Nanoscale*, 2009, **1**, 16-39.
38. Z. Gu, Y. Yong, L. Zhou, L. Yan, G. Tian, X. Zheng, X. Liu, X. Zhang, J. Shi, W. Cong, W. Yin and Y. Zhao, *Nanoscale*, 2014, ***6***, 10394-10403.
39. X. H. Gao, Y. Y. Cui, R. M. Levenson, L. W. K. Chung and S. M. Nie, *Nat. Biotechnol.*, 2004, **22**, 969-976.
40. V. Wagner, A. Dullaart, A. K. Bock and A. Zweck, *Nat. Biotechnol.*, 2006, **24**, 1211-1217.
41. S. Mura, J. Nicolas and P. Couvreur, *Nat. Mater.*, 2013, **12**, 991-1003.
42. Slowing, II, J. L. Vivero-Escoto, C. W. Wu and V. S. Y. Lin, *Adv. Drug Deliv. Rev.*, 2008, **60**, 1278-1288.
43. M. Ferrari, *Nat. Rev. Cancer*, 2005, **5**, 161-171.
44. Y. Sun, Y. Zheng, H. Ran, Y. Zhou, H. Shen, Y. Chen, H. Chen, T. M. Krupka, A. Li, P. Li, Z. Wang and Z. Wang, *Biomaterials*, 2012, **33**, 5854-5864.
45. C. Niu, Z. Wang, G. Zuo, T. M. Krupka, H. Ran, P. Zhang, P. Li, Y. Chen, H. Chen and Y. Zheng, *Clin Breast Cancer*, 2012, **12**, 199-206.
46. C. Niu, Z. Wang, G. Lu, T. M. Krupka, Y. Sun, Y. You, W. Song, H. Ran, P. Li and Y. Zheng, *Biomaterials*, 2013, **34**, 2307-2317.
47. A. K. Gupta and M. Gupta, *Biomaterials*, 2005, **26**, 3995-4021.
48. X. Feng, F. Gao and Y. Zheng, *Opt Lett*, 2014, **39**, 3414-3417.
49. L. Xi, S. R. Grobmyer, G. Zhou, W. Qian, L. Yang and H. Jiang, *J Biophotonics*, 2014, **7**, 401-409.
50. L. Xi, M. Satpathy, Q. Zhao, W. Qian, L. Yang and H. Jiang, *Nanomedicine*, 2014, **10**, 669-677.
51. Y. Zhou, Z. Wang, Y. Chen, H. Shen, Z. Luo, A. Li, Q. Wang, H. Ran, P. Li, W. Song, Z. Yang, H. Chen, G. Lu and Y. Zheng, *Adv. Mater.*, 2013, **25**, 4123-4130.
52. H. Cao, Z. Xu, H. Long, L. L. Zhang, J. Zhang, Z. P. Peng and S. L. Li, *Ultrasound Med. Biol.*, 2011, **37**, 1009-1016.

53. Q. Li, Y. B. Xiao, Z. G. Liang, J. Y. Chen and Z. B. Wang, *Ultrasound Med. Biol.*, 2012, **38**, 1576-1581.
54. C. Li, W. Zhang, R. Zhang, L. Zhang, P. Wu and F. Zhang, *Eur. J. Cancer*, 2010, **46**, 2513-2521.
55. J. A. Kopechek, E. Park, C. S. Mei, N. J. McDannold and T. M. Porter, *J. Healthc. Eng.*, 2013, **4**, 109-126.
56. L. C. Phillips, C. Puett, P. S. Sheeran, G. Wilson Miller, T. O. Matsunaga and P. A. Dayton, *J. Acoust. Soc.Am.*, 2013, **134**, 1473-1482.

Figures and captions

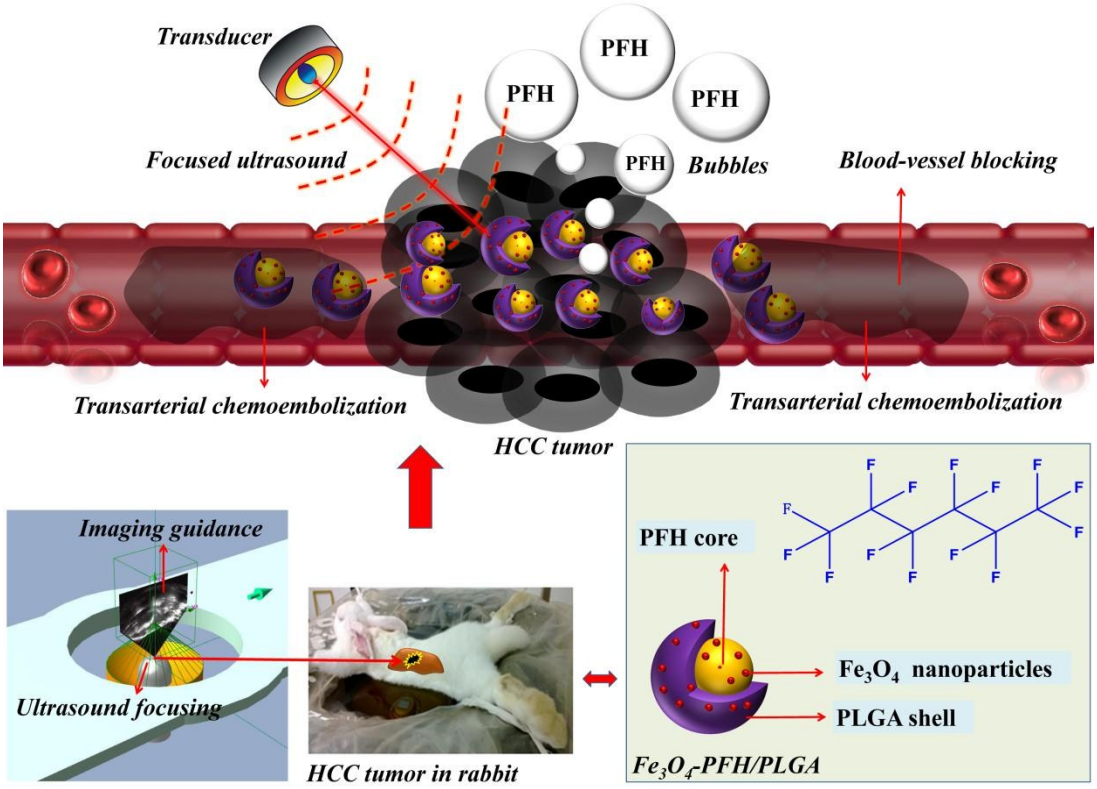

Scheme 1. Schematic illustration of the transarterial chemoembolization enhancing the nanoparticle-based synergistic cancer (HCC) surgery of HIFU and the microstructure of Fe_3O_4-PFH/PLGA composite nanocapsules.

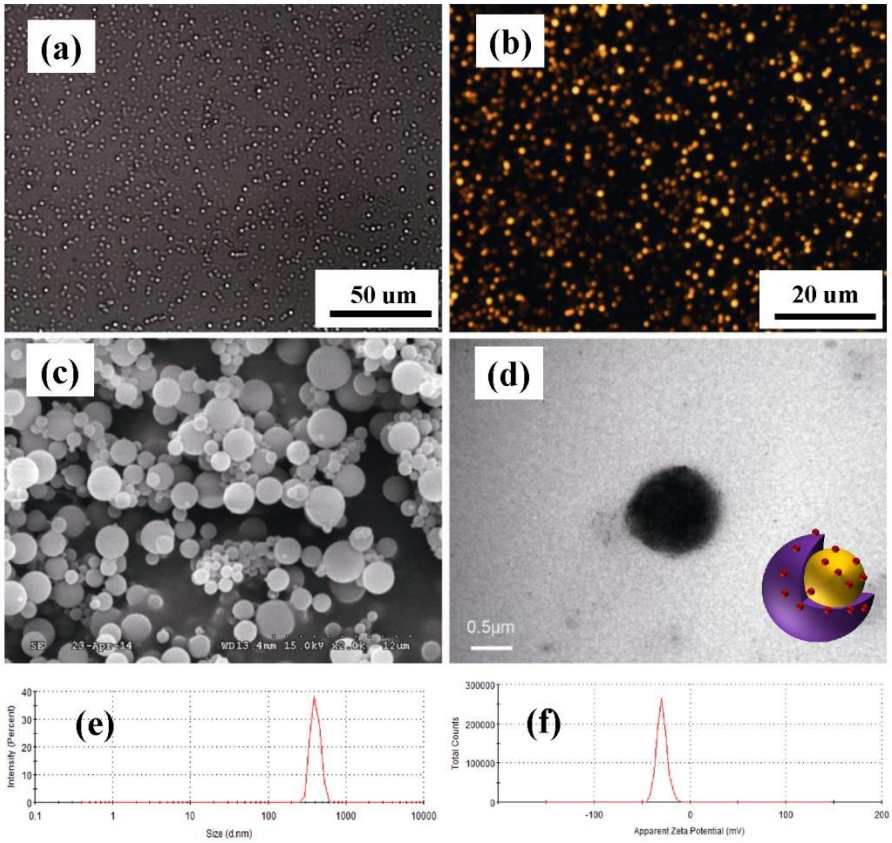

Figure 1. (a) Bright-field optical-microscopic image of Fe_3O_4-PFH/PLGA composite nanocapsules. (b) Confocal laser scanning microscopic (CLSM) image of DiI dye-loaded Fe_3O_4-PFH/PLGA nanocapsules. (c) SEM and (d) TEM image of Fe_3O_4-PFH/PLGA nanocapsules, and their corresponding (e) dynamic light scattering and (f) Zeta potential curves.

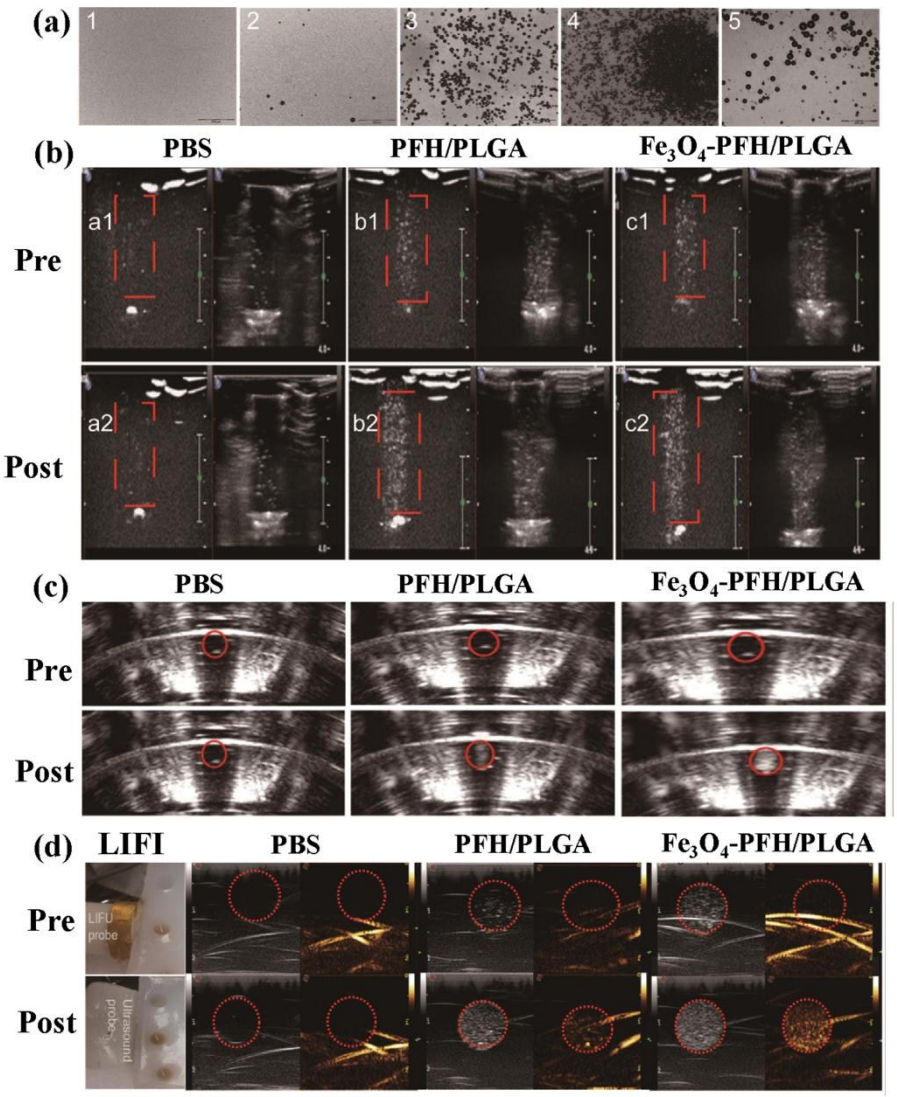

Figure 2. (a) Bright-field optical-microscopic images of Fe_3O_4-PFH/PLGA nanocapsules after heating to different temperatures (56 ℃ (1), 64 ℃ (2), 70 ℃ (3), 80 ℃ (4) and 90 ℃ (5)). (b) B-mode and contrast-mode ultrasound images of Fe_3O_4-PFH/PLGA, PFH/PLGA and PBS before (a_1, b_1 and c_1) and after (a_2, b_2 and c_2) heating to 70 ℃. (c) The gray-scale changes of PBS, PFH/PLGA, Fe_3O_4-PFH/PLGA before and after HIFU exposure at the condition of irradiation power of 150 W and irradiation duration of 5s. (d) Ultrasound images at B mode and contrast model of PBS, PFH/PLGA, Fe_3O_4-PFH/PLGA before and after LIFU exposure at the condition of irradiation power of 8 W and irradiation duration of 30 s.

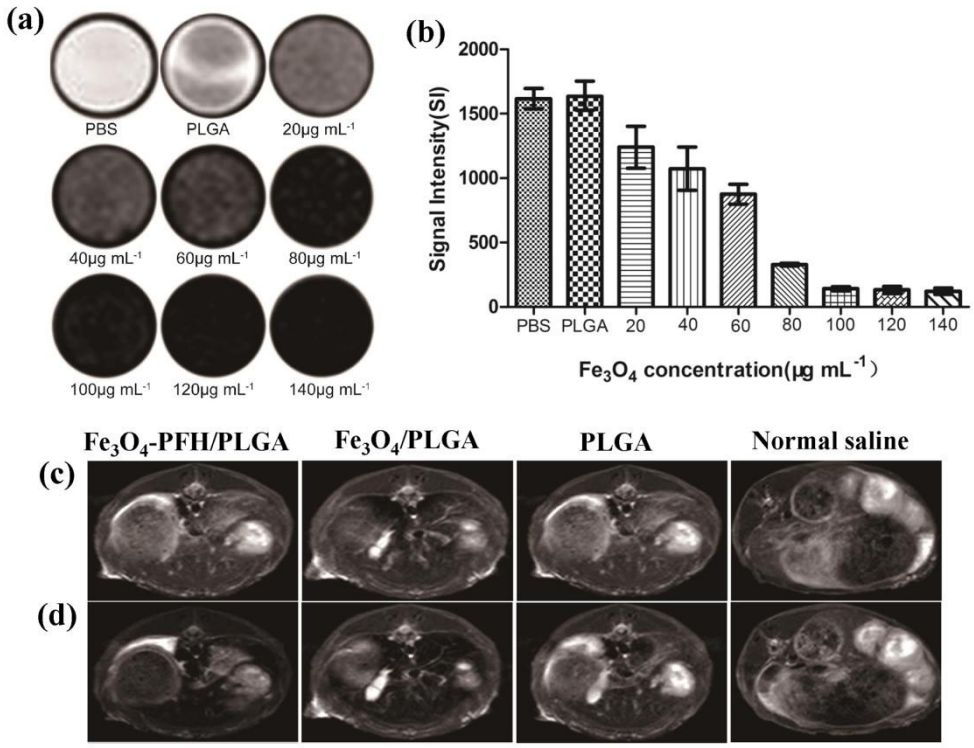

Figure 3. (a) *In vitro* T_2-weighted MR images and (b) MRI signal intensities of the Fe_3O_4/PLGA nanocapsule solution at different Fe concentrations (20, 40, 60, 80, 100, 120, 140 μg/ml) , PBS and pure PLGA nanospheres as the contrast agents. *In vivo* T_2-weighted MR imaging of HCC tumor in liver of rabbits (c) before and (d) after the intravenous administration of normal saline, PLGA, Fe_3O_4/PLGA and Fe_3O_4-PFH/PLGA. The images were acquired immediately after the administration of various agents.

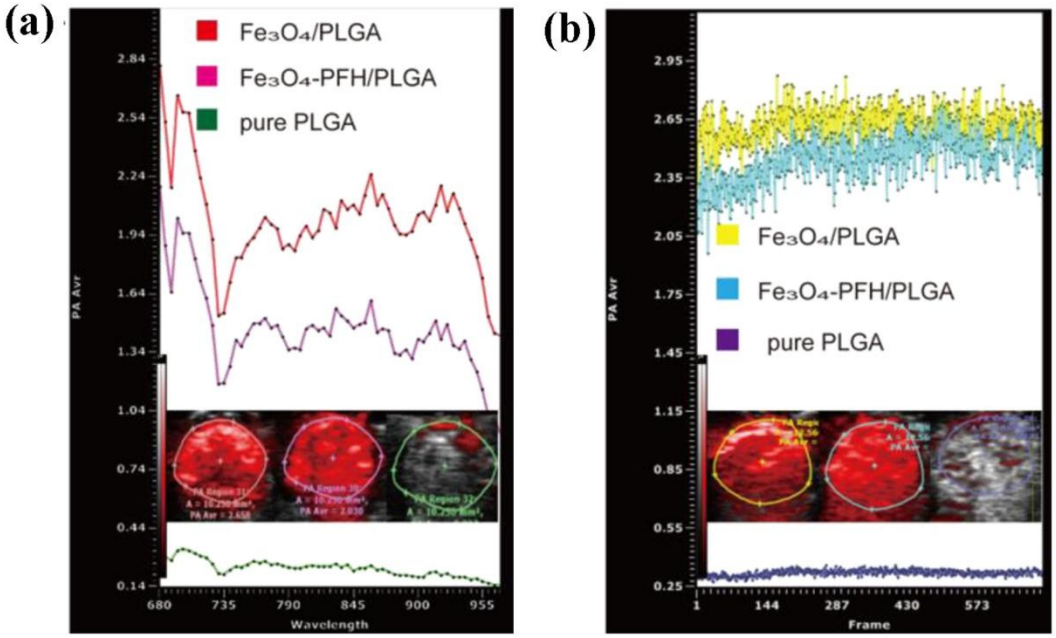

Figure 4. (a) PA signal curve of Fe_3O_4/PLGA, Fe_3O_4-PFH/PLGA and pure PLGA at the same concentration (100 mg/mL) at 680 nm-955 nm Laser irradiation. (b) PA intensity changes of Fe_3O_4/PLGA, Fe_3O_4-PFH /PLGA and pure PLGA at the time (0.2 s/Frame) of laser irradiation at 695 nm.

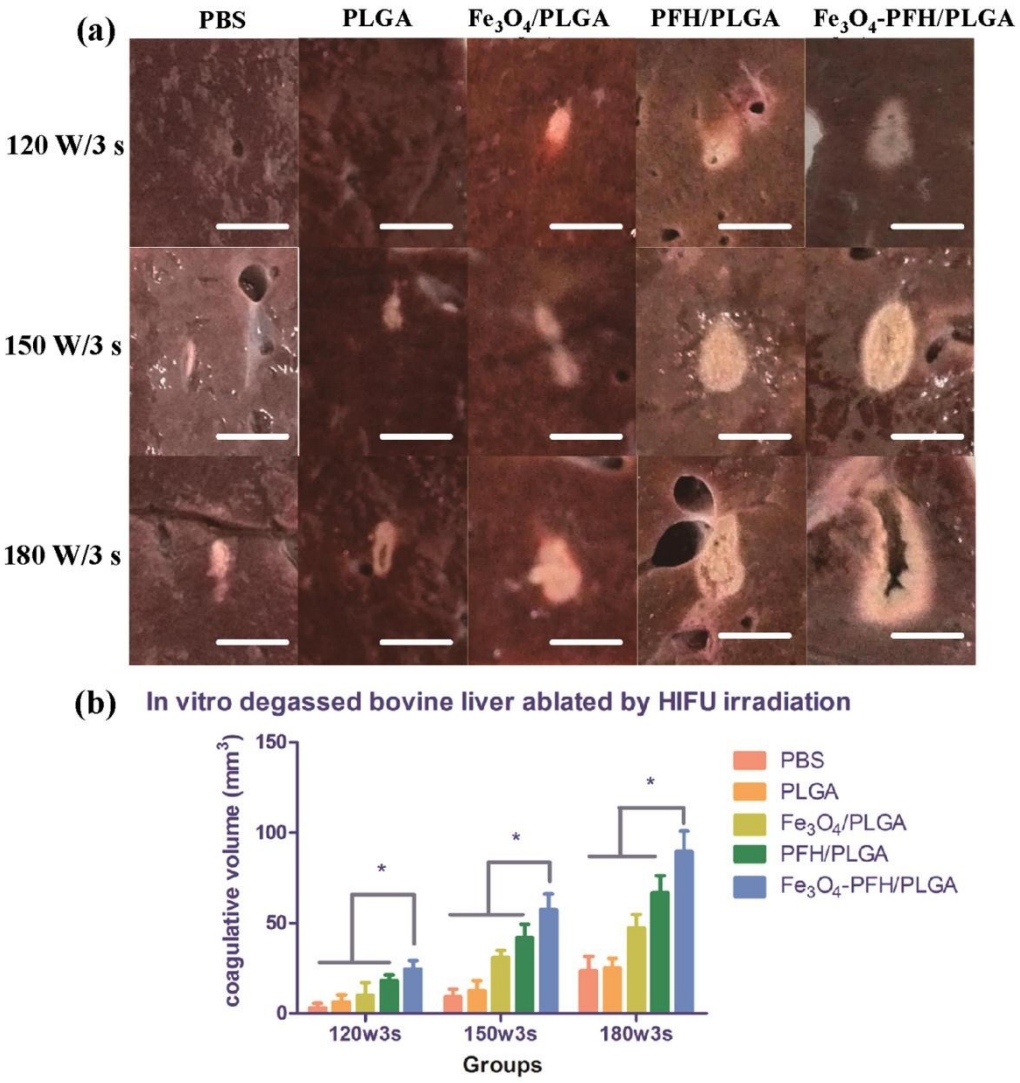

Figure 5. (a) *Ex vivo* macroscopic image of bovine liver exposure to HIFU ablation after the intra-tissue injection of different agents, including PBS, pure PLGA, Fe_3O_4/PLGA, PFH/PLGA and Fe_3O_4-PFH/PLGA. The HIFU irradiation condition includes 120 w/3 s, 150 w/3 s and 180 w/3 s, respectively. (b) The coagulation volume degassed bovine liver after the injection of PBS, pure PLGA, Fe_3O_4/PLGA, PFH/PLGA and Fe_3O_4-PFH /PLGA and exposure to HIFU irradiation at different conditions. The coagulation volumes of the groups of Fe_3O_4-PFH/PLGA and PFH/PLGA were signally larger than other three groups (*P <0.05). The scale bar is 1 cm for all images.

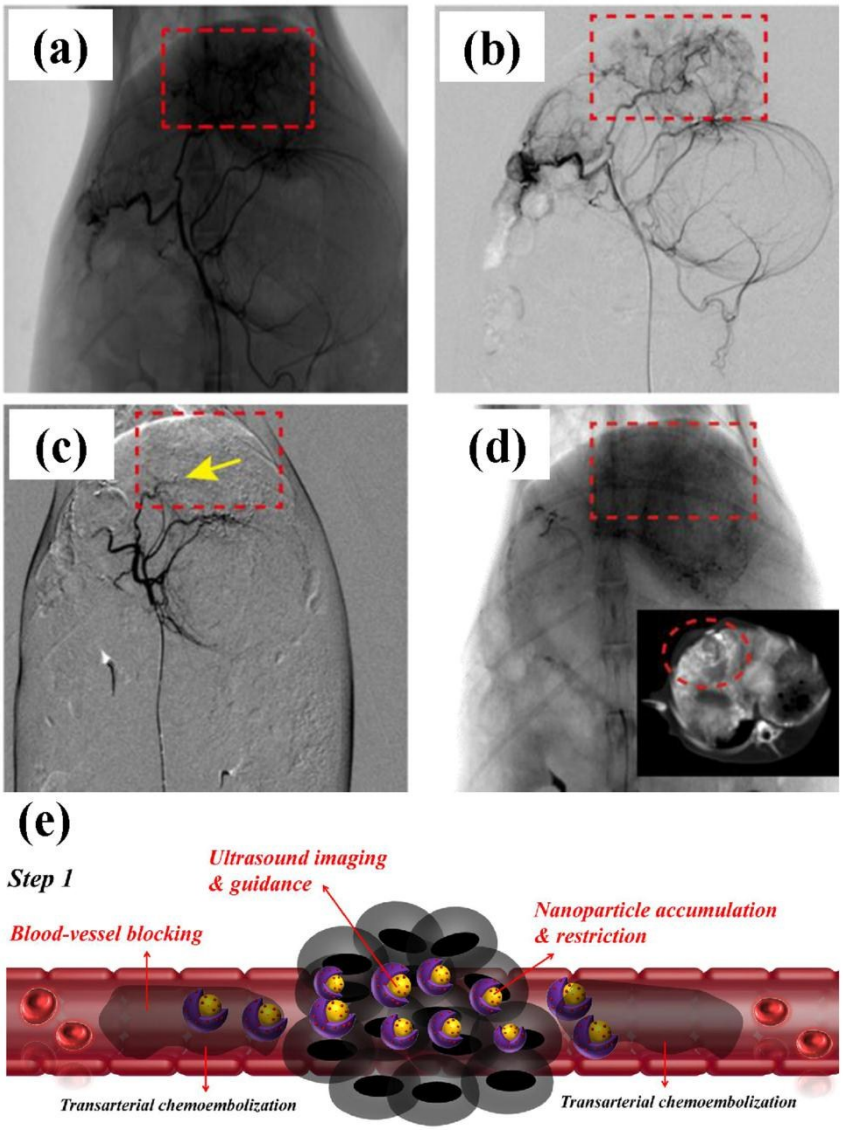

Figure 6. (a) Rabbit hepatic angiographic image. (b) Digital X-ray inspectoscope image after the injection of Fe_3O_4-PFH/PLGA and Lipiodol concurrently. (c) DSA image after perfusion of complex emulsion. The tumor vessels were occluded and disappeared on the image (yellow arrow). (d). Digital X-ray inspectoscope image and CT image (inset image) after transarterial injection of Fe_3O_4-PFH/PLGA and Lipiodol emulsion. The emulsion deposited in the VX2 tumor area. (e) Schematic illustration of the blood-vessel blocking by Lipiodal after transarterial chemoembolization to enhance the accumulation and retention of Fe_3O_4-PFH/PLGA within tumor tissues.

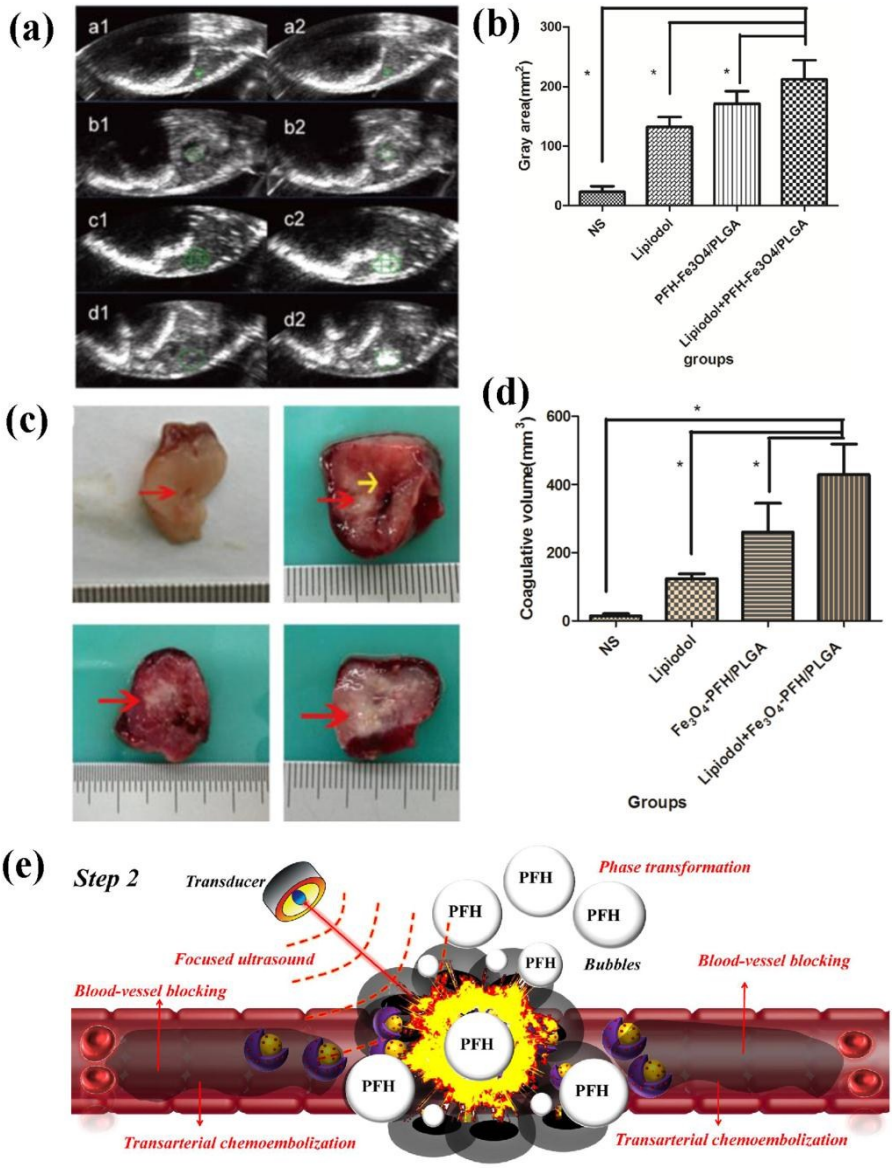

Figure 7. (a) *In vivo* ultrasound image VX2 hepatic carcinoma in rabbits before (a_1, b_1, c_1 and d_1) and after (a_2, b_2, c_2 and d_2) the administration of normal saline, Lipiodol, Fe_3O_4-PFH/PLGA and Lipiodol combined with Fe_3O_4-PFH/PLGA. (b) The gray-area calculation based on the ultrasound imaging of each treatment group. (c) Digital picture of *ex vivo* VX2 hepatic carcinoma showing the HIFU ablation volume of each treatment group. (d) The calculated coagulation volume of VX2 hepatic carcinoma after the HIFU treatments (*P < 0.05). (e) Schematic illustration of the accumulation of Fe_3O_4-PFH/PLGA within tumor tissue assisted by Lipiodol to block the blood vessel, phase changing of PFH core upon HIFU irradiation and subsequent tumor-tissue ablation.

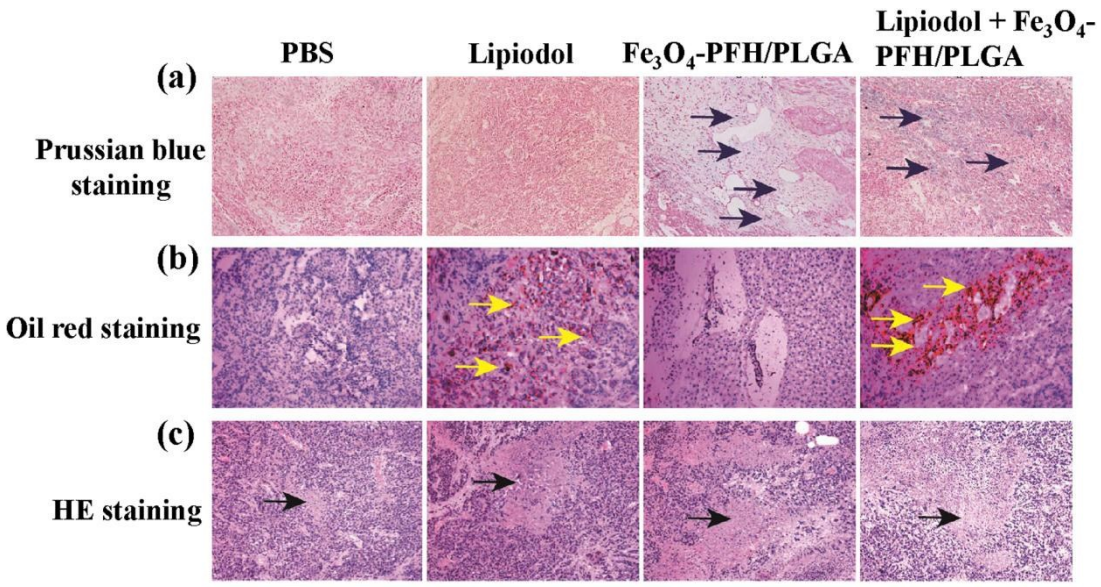

Figure 8. (a) Microscopic image of tumor tissues from different groups after Prussian blue staining. The iron element in the Fe_3O_4-PFH/PLGA and Lipiodol combined with Fe_3O_4-PFH/PLGA groups of liver tissue slices was stained blue (blue arrow). No blue staining was observed in the normal saline and Lipiodol groups (×100 magnification). (b) Microscopic image of oil red staining in liver tissue. Lipiodol from the Lipiodol and Lipiodol combined with Fe_3O_4-PFH/PLGA groups of liver tissue slices was stained red (yellow arrow). No red staining was observed in the normal saline and Fe_3O_4-PFH/PLGA groups (×100 magnification). (c) HE staining of the tumor-tissue sections after HIFU treatment (×100 magnification). The larger ablation area appeared in Lipiodol combined with Fe_3O_4-PFH/ PLGA groups (×100 magnification, black arrow express ablation area).

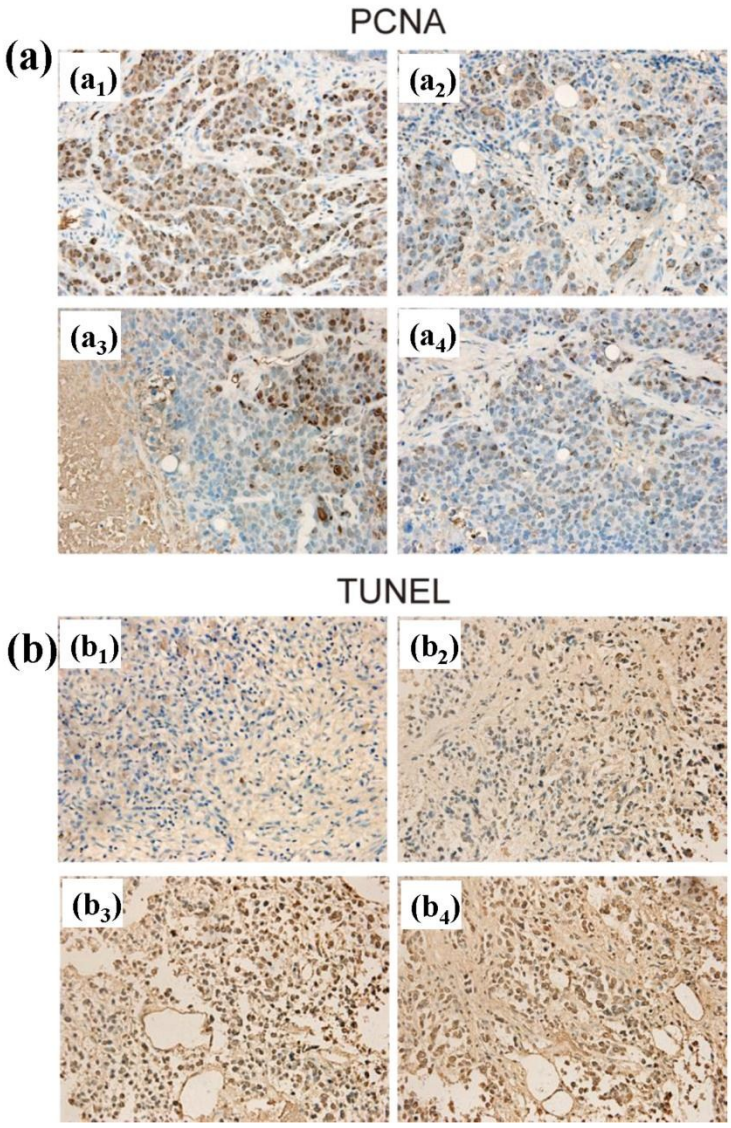

Figure 9. The expression of (a) PCNA and (b) TUNEL in tumor tissue by immunohistochemical examination. (a_1 and b_1) saline group, (a_2 and b_2) Lipiodol group, (a_3 and b_3) Fe_3O_4-PFH /PLGA group, (a_4 and b_4) Lipiodol combined with Fe_3O_4-PFH/PLGA group. The nucleus appearing brown was PCNA-positive or TUNEL-positive cell, and the blue represents the negative cells (×400 magnification).

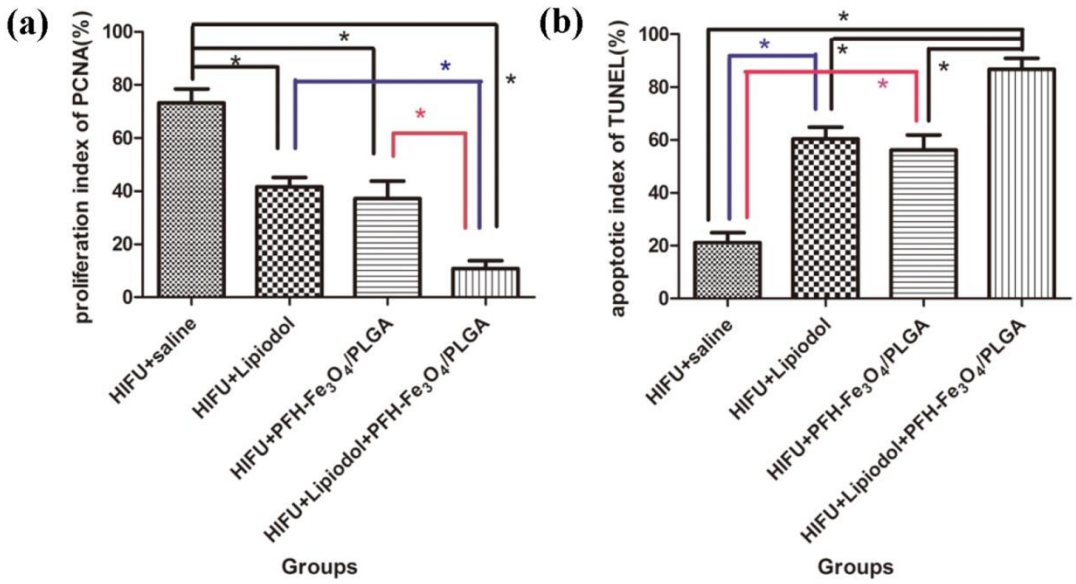

Figure 10. (a) The proliferative index (PI) of PCNA and (b) apoptotic index (AI) of TUNEL in each group (*P < 0.05). These two figures showed that the Lipiodol combined with Fe_3O_4-PFH/PLGA group caused significantly lower PI and higher AI than that of other three groups. The Lipiodol group and Fe_3O_4-PFH/PLGA group had lower PI and higher AI than normal saline group (blue and red line respectively,*P < 0.05), and there was no obvious difference between Lipiodol group and Fe_3O_4-PFH /PLGA group (*P > 0.05).